

Hard Magnets after Freezing of Spin Dynamics of Soft Magnets in Cobalt(II)–Radical Chain Compounds

Yoshitomo Okamura, Norio Ishii, Takashi Nogami, and Takayuki Ishida*

Department of Applied Physics and Chemistry, The University of Electro-Communications, Chofu, Tokyo 182-8585

Received November 30, 2009; E-mail: ishi@pc.uec.ac.jp

Several metal–radical alternating chains ([Co(hfac)$_2$(C$_n$PNN)]) were prepared, and their crystal structures and magnetic properties were systematically studied, where C$_n$PNN stands for a phenylnitronyl nitroxide ligand having a linear C$_n$ alkoxy group at the ortho or para position. X-ray crystal structure analysis was successfully performed for [Co(hfac)$_2$(*p*-C$_5$PNN)] (**p-5**). The chain structure is similar to those of the known *p*-butoxy and *o*-ethoxy derivatives. Compound **p-5** showed a very large coercive field of 51 kOe (4.1 MA m^{-1}) and a saturation magnetization of 9.7×10^3 erg Oe^{-1} mol^{-1} at 6 K. *o*-Propoxy and *o*-pentoxy derivatives also exhibited large coercive fields of 50–54 kOe at 5–6 K. The activation energies of magnetization reorientation for the present compounds were estimated to be as large as 290–360 K from Arrhenius analysis using ac susceptibility data. In a temperature range of ca. 10–40 K, all of the present compounds behaved as very soft magnets, as indicated by no hysteresis in the ferromagnetic *M*–*H* curves. We propose a mechanism for the drastic soft–hard switch. The hard character grows immediately after freezing of the spin dynamics owing to the strong magnetic anisotropy.

A variety of low dimensional complexes containing nitronyl nitroxide (NN) radicals[1] with metal 1,1,1,5,5,5-hexafluoropentane-2,4-dionate (hfac) salts have been extensively studied in pursuit of metal–radical hybrid magnets[2] (the systematic name of NN is 4,4,5,5-tetramethylimidazoline-1-oxyl 3-oxide). Since the discovery of the first single-chain magnet (SCM) [Co^{II}(hfac)$_2$(*p*-C$_1$PNN)] by Gatteschi et al.[3,4] (abbreviated as **p-1** hereafter; for the molecular structure, see Figure 1a with R = CH$_3$), several derivatives containing smaller ligands[5] and 4f-metal ions[6] and other systems[7,8] have been investigated toward novel SCMs. Intermolecular interaction among single-molecule magnets (SMMs) have been discussed for a dimer of the [Mn$_4$]-based SMM.[9] Similarly, there seems to be a chance to introduce interchain interaction to SCM systems, because various [M^{II}(hfac)$_2$(RNN)] chains exhibited magnetic ordering,[2,10–14] though the SCM character has been supposed to be incompatible with the bulk magnetic phenomena.[4,7,8] We have found interplay between SCM and bulk characters in [Co^{II}(hfac)$_2$(*p*-C$_4$PNN)] (**p-4**).[15,16] Most interestingly, **p-4** showed the record coercivity of 52 kOe at 6 K. The long-range order of **p-4** has been confirmed by zero-field muon spin rotation/relaxation study.[16] We have also presented the ortho-substituted derivative [Co^{II}(hfac)$_2$(*o*-C$_2$PNN)] (**o-2**; R = C$_2$H$_5$ in Figure 1b) showing a comparably large coercivity (54 kOe at 6 K).[17]

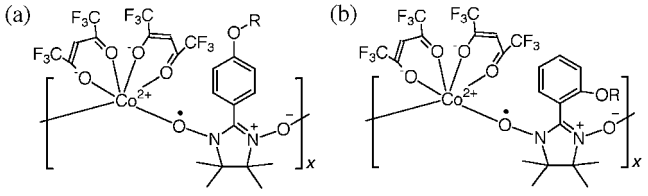

Figure 1. (a) Para- and (b) ortho-derivatives of [Co(hfac)$_2$-(C$_n$PNN)].

To investigate the relationship between the magnetic properties and crystal structures, we have prepared several related compounds consisting of C$_n$PNN and [Co(hfac)$_2$]. A para-derivative, **p-5**, has been newly prepared and proven to exhibit a very wide hysteresis just like **p-4** and not like **p-1**. Some ortho-derivatives have also been investigated. Such examples have potential as a general synthetic path to obtain magnets with large coercivity. The magnetic anisotropy observed may provide a clue to the mechanism of the hardness of these magnets. We will propose a possible mechanism and discuss what happens at the critical temperature of the hard magnet phase.

Results and Discussion

Preparation and Structural Characterization. Complexations of [Co(hfac)$_2$] with paramagnetic bridging ligands (*o*- and *p*-C$_n$PNN) were conducted in heptane–dichloromethane according to conventional methods.[2,4,15] The products were obtained as bluish purple fine needles or powder. The crystal structures of **p-4**, **p-5**, and **o-2** have been successfully determined (Table 1). The specimen of **p-2**, **p-3**, **o-3**, **o-4**, or **o-5** did not afford good crystals for X-ray diffraction study. We tried complexations using meta-derivatives, but the resultant compounds were not suitable for further structural or magnetic study. In some cases, the meta-radical precursors are oily, and accordingly the characterization of the [Co(hfac)$_2$] complexes were less reliable than the ortho- and para-derivatives because of the difficulty of preparation.

As Figure 2a shows, there are two crystallographically independent units in the unit cell of **p-5**, each of which is arranged to form a metal–radical alternating chain running along the crystallographic *b* axis with a 2_1 screw symmetry. The space group is $P2_1/n$. The geometric features are similar to

Published on the web May 28, 2010; doi:10.1246/bcsj.20090316

Table 1. Selected Crystallographic Data for **p-5**, **p-4**, and **o-2**

	Compounds		
	p-5	**p-4**	**o-2**
Formula	$C_{28}H_{29}CoF_{12}N_2O_7$	$C_{27}H_{27}CoF_{12}N_2O_7$	$C_{25}H_{23}CoF_{12}N_2O_7$
Crystal system	monoclinic	monoclinic	monoclinic
Space group	$P2_1/n$	$P2_1/n$	$P2_1/n$
a/Å	21.987(11)	21.7966(8)	11.084(3)
b/Å	14.010(9)	14.0889(4)	13.954(4)
c/Å	22.430(10)	22.0906(6)	20.209(6)
β/°	109.58(4)	111.2626(9)	97.566(3)
V/Å^3	6510(6)	6322.0(3)	3098.5(15)
Z	8	8	4
d_{cal}/g cm^{-3}	1.617	1.636	1.608
μ(Mo Kα)/mm^{-1}	0.643	0.661	0.671
R_{int}	0.119	0.083	0.120
$R(F)$[a] ($I > 2\sigma(I)$)	0.0698	0.0436	0.0847
$R_w(F^2)$[b] (all data)	0.1230	0.0631	0.2233
G. O. F.	0.966	1.046	0.904
Unique reflections	12829	14028	6667
T/K	108	100	100
Reference	this work	Ref. 15	Ref. 17

a) $R = \Sigma\ ||F_o| - |F_c||/\Sigma\ |F_o|$. b) $R_w = [\Sigma\ w(F_o^2 - F_c^2)^2/\Sigma\ w(F_o^2)^2]^{1/2}$.

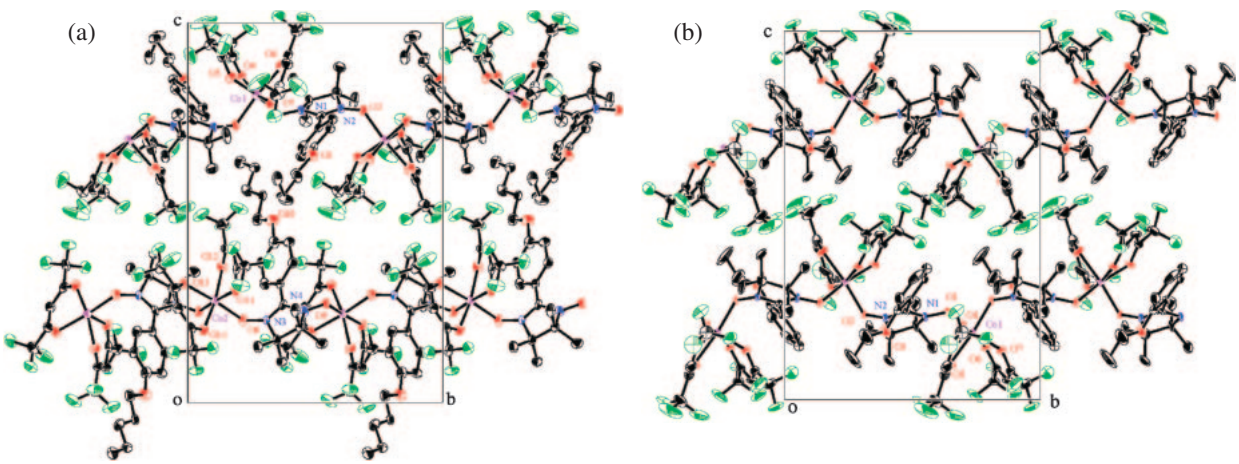

Figure 2. Crystal structures of (a) **p-5** and (b) **o-2** viewed along the crystallographic a axis. Thermal ellipsoids are drawn at the 50 and 30% probability levels for (a) and (b), respectively. Selected atoms are numbered. Hydrogen atoms are omitted. Four formula units are shown in each chain.

each other except for the conformation at the pentyl side chains; trans-zigzag for the Co2 chain (shown in the bottom portion of Figure 2a) and partly gauche for the Co1 chain (in the top portion). The radical oxygen atoms are located in a cis manner around the Co ions (the O1–Co1–O2$^{\#}$ and O8–Co2–O9* angles are 83.4(2) and 82.9(2)°, respectively, where the symmetry operation codes of $^{\#}$ and * are $1/2 - x$, $-1/2 + y$, $3/2 - z$, and $1/2 - x$, $-1/2 + y$, $1/2 - z$, respectively). The intrachain Co···Co distances are 7.5064(15) and 7.3833(15) Å for the Co1 and Co2 chains, respectively. The magnetic properties imply the sum of the two kinds of chains. The interchain Co···Co distances are 10.41 Å and larger, and thus the interchain couplings are smaller than the intrachain ones.

The molecular and crystal structures of **p-5** are quite similar to those of **p-4**.[15] Owing to an additional CH_2 group in **p-5**, the cell volume of the crystal of **p-5** is 3.0% larger than that of **p-4**. We could not obtain so far any large single crystal of **p-5** suitable for the study of magnetic anisotropy, but we safely expect that the magnetic anisotropy of **p-5** would be similar to that of **p-4** from the isomorphism between them.

Compound **o-2** also crystallized in a monoclinic $P2_1/n$ space group.[17] The crystal structure is shown in Figure 2b for comparison. There are two chains in the crystal lattice of **o-2**, but they are symmetrically correlated. The a length and the cell volume are approximately half of those of **p-5** and **p-4**. Each chain has a 2_1 screw symmetry in the crystallographic b axis, with a cis-zigzag configuration (the O1–Co1–O2† angle is 81.3(2)°, where the symmetry operation code of † is $1/2 - x$, $1/2 + y$, $1/2 - z$). The intrachain Co1···Co1† distance is 7.5177(14) Å. The local geometry around the cobalt ion is comparable to those of **p-4** and **p-5**.

At this stage, it is concluded that the packing motifs of the one-dimensional chains in the crystal are somewhat different among the para- and ortho-derivatives, but that the polymer backbone structures are quite similar to each other. Striking difference was found between **o-1** and the present compounds; the crystal of **p-1** has been reported to possess a 3_1 helical symmetry in a trigonal $P3_1$ space group,[4] whereas the crystals of **p-5**, **p-4**, and **o-2** have a 2_1 helical symmetry in a monoclinic lattice. The magnetic easy and hard axes were determined by using their single crystals, and we also found difference between the directions of the easy axis (see below).

Compounds **o-3** and **o-5** did not afford single crystals suitable for X-ray crystallographic analysis. The powder XRD of **o-2**, **o-3**, and **o-5** were quite similar to each other (Figure 3). Furthermore, they are also similar to those of **p-4** and **p-5**. The para-derivatives possess two independent chains in the unit cell, but the difference between the structures of two chains seems trivial, that is the twofold structure of **p-4** and **p-5** would cause satellite peaks, which were weak or mostly extinct in the XRD. Thus, the para- and ortho-derivatives can be regarded as approximate isomorphs.

The peak at $2\theta = 8.60°$ of **o-2** is assigned to the $1\,0\,-1$ reflection and the Bragg condition gave $d = 10.3$ Å. The corresponding peaks of **o-3** and **o-5** gave $d = 10.5$ and 10.8 Å, respectively. The unit cells become larger with an increase of the alkyl chain length. We found a somewhat different powder XRD profile for **o-4** (not shown), implying that the crystal structure of **o-4** is different from those of **o-2**, **o-3**, and **o-5**. The results of **o-4** are omitted in further description and discussion. Since the crystal structures of **p-4**, **p-5**, and **o-2** have been determined, we will describe in detail on the physical properties of **p-5** and **o-2** hereafter, in comparison with those of **p-4**.

Magnetic Properties of the Para-Derivatives. We measured the static molar magnetic susceptibility (χ_{mol} on the repeating unit basis) on polycrystalline specimens of the present compounds with a static magnetic field of 500 Oe. The temperature dependence of $\chi_{mol}T$ for **p-5** (Figure 4a) showed an upsurge from 2.71 $cm^3\,K\,mol^{-1}$ at 300 K to 134 $cm^3\,K\,mol^{-1}$ at 43 K on cooling, clearly indicating the ferrimagnetic spin alignment within a chain, as usually observed for $[Co(hfac)_2(RNN)]$-type polymers.[2,4,5] We applied the Curie–Weiss law, $\chi_{mol} = C/(T-\theta)$, to the χ_{mol}^{-1} vs. T plot in a temperature range of 100–300 K, giving $C = 1.900 \pm 0.010\,cm^3\,K\,mol^{-1}$ and $\theta = +87.2 \pm 0.7$ K. The θ value implies empirical meaning because interchain interaction would be present (see below) together with the intrachain ferrimagnetic behavior. The data at lower temperatures did not obey the Curie–Weiss low, as indicated with an abrupt drop in the $\chi_{mol}T$ vs. T plot, mainly because of a saturation effect. Bulk magnetic properties of **p-5** were confirmed by the following experiments.

As Figure 4b shows, the FCM (field-cooled-magnetization) of **p-5** gradually increased around 60 K, formed a shoulder near

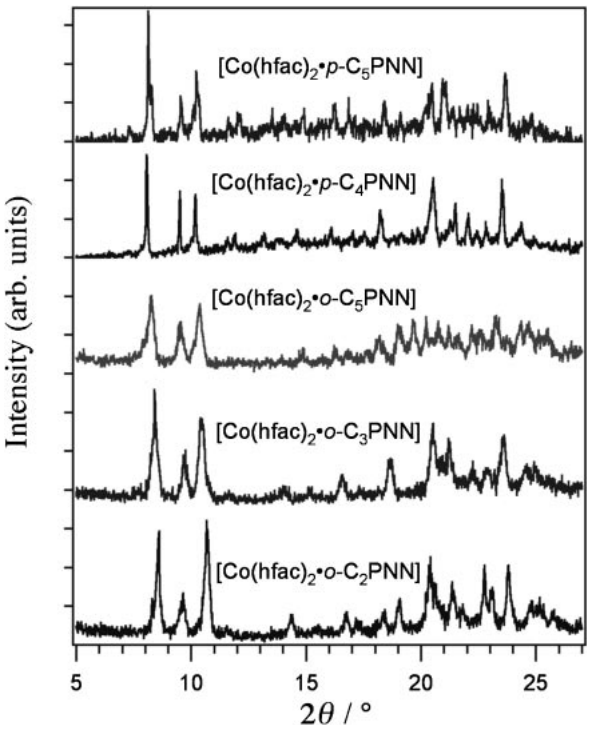

Figure 3. XRD profiles of **p-5**, **p-4**, **o-5**, **o-3**, and **o-2**.

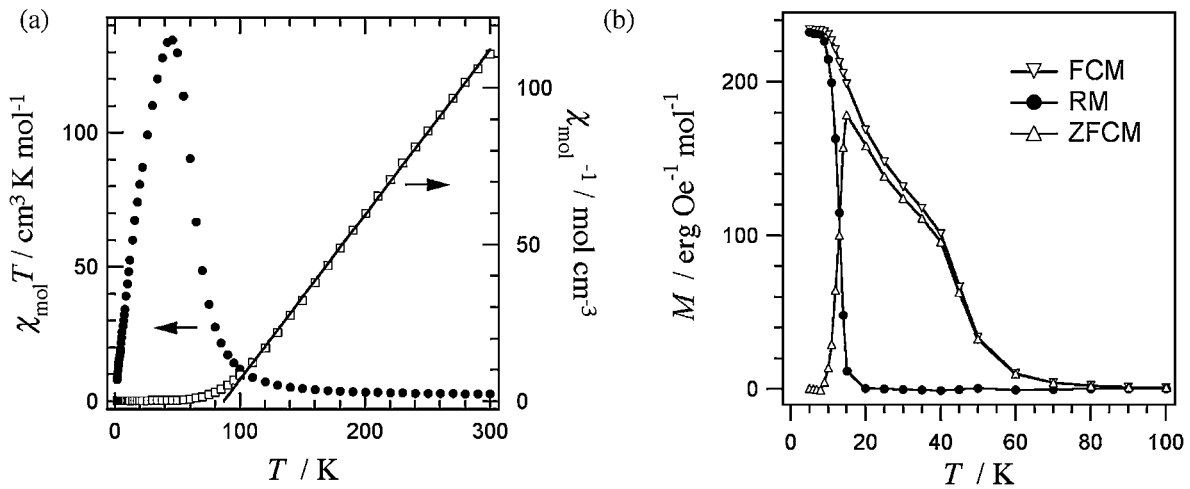

Figure 4. (a) The $\chi_{mol}T$ vs. T and χ_{mol}^{-1} vs. T plots for randomly oriented polycrystalline **p-5** with an applied field of 500 Oe. The Curie–Weiss analysis is indicated with a solid line. (b) FCM, RM, and ZFCM for randomly oriented polycrystalline **p-5** with an applied field of 5 Oe for FCM and ZFCM.

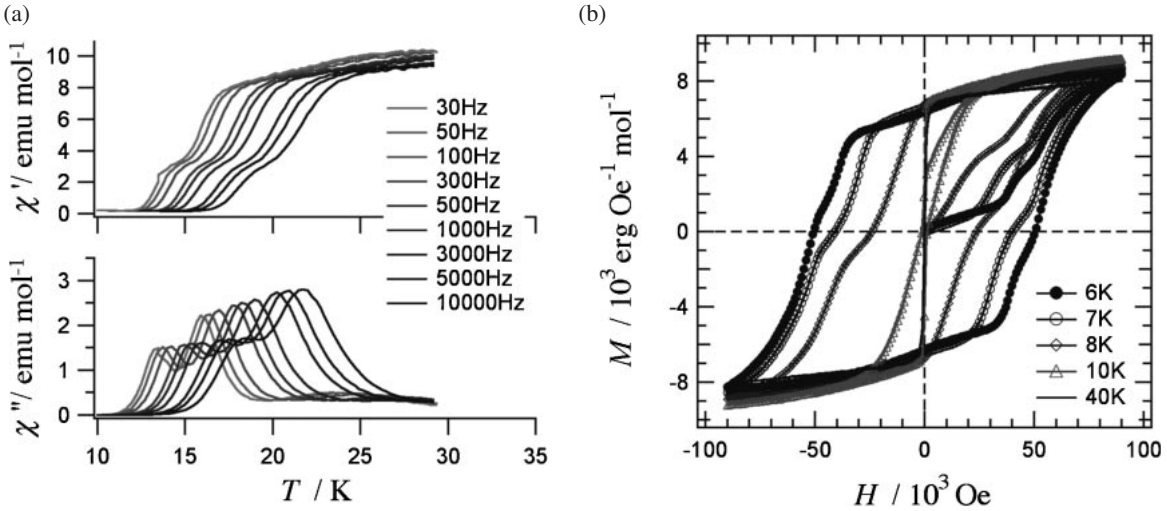

Figure 5. (a) In-phase and out-of-phase ac magnetic susceptibilities, χ' and χ'', respectively, of polycrystalline **p-5** as a function of temperature and frequency. The ac field amplitude was 5 Oe. (b) Hysteresis loops of polycrystalline **p-5** measured at 6, 7, 8, 10, and 40 K. The field scan rate was almost constant at 18 Oe s^{-1}.

40 K, and finally reached a saturation value at 10 K. The RM (remnant magnetization) did not change below 10 K, but rapidly decayed at 10 K on warming. The ZFCM (zero-field-cooled magnetization) curve started to increase at 10 K on heating. Below 10 K, appreciable discrepancy was observed between the FCM and ZFCM curves, and the RM remained. Usually this is referred to as being magnetically "hard,"[18] and may be potentially utilized for permanently magnetized materials with strong hysteresis. As for conventional bulk magnets, the critical temperature T_C or T_N could be defined as the temperature where RM disappears. In the present case however, this behavior is accompanied by the slowing-down of the dynamics of magnetization reorientation, as revealed by the ac susceptometry (see below), and therefore this specimen is not a magnet of conventional definition.

In 10–ca. 40 K, **p-5** was very sensitively magnetized, suggesting a long-range ferromagnetic character. The chain has a ground ferrimagnetic state,[2,4,5] and accordingly the ferromagnetic character should be attributed to the interchain coupling. At the same time, **p-5** was ready to lose the RM, and the FCM and ZFCM curves were practically identical. This finding implies the absence of hysteresis. Such ferromagnetic materials are said to be magnetically "soft."[18] They have high permeability but very small coercivity, and therefore have very narrow hysteresis loops in general. Thus, the critical behavior around 10 K is best expressed in terms of a drastic "soft–hard switch," which has originally been proposed for **p-4**.[15]

One may wonder whether the state in 10–ca. 40 K would be a merely short-range ordered state, but this possibility is eliminated by the μSR experiments on **p-4**.[16] Compound **p-4** enters into the static magnetically ordered state below 40 K. The magnetic hardness is related to the dynamics of domain wall movement. It should be emphasized that the crystal structure and magnetic properties of **p-5** are almost identical to those of **p-4**.

We examined the magnetic anomaly just above 10 K for **p-5**. Figure 5 displays a remarkable frequency dependence of the ac magnetic susceptibility (χ' and χ''). There are two χ'' peaks and concomitant χ' shoulders. We checked in detail repeated measurements of several single crystals selected and manually aligned under a microscope, giving complete reproducibility with a constant relative ratio between the two signals. This finding is compatible with the fact that there are two independent chains in the unit cell of **p-5**.

The frequency dependence of peak or shoulder temperatures (T_p) in χ' was analyzed according to the equation $\phi = (\Delta T_p/T_p)/\Delta(\log\omega)$, and in the present case the ϕ values were calculated to be 0.115 ± 0.003 and 0.113 ± 0.005 for the low- and high-temperature signals, respectively. This finding excludes possibility of a spin-glass state ($0.01 < \phi < 0.08$).[19] The relaxation rate ($k = 1/\tau$) is equal to the frequency of the applied ac field ($2\pi\nu$) at the temperature of the maximum of χ''. The effective energy barrier (E_a) of the magnetization reorientation was estimated on the basis of the Arrhenius-law,[7,20,21] $\ln 2\pi\nu = -\ln\tau_0 - E_a/k_BT$, giving $E_a/k_B = 290 \pm 3$ K and $\tau_0 = (2.15 \pm 0.45) \times 10^{-12}$ s for the low-temperature signal and $E_a/k_B = 350 \pm 5$ K and $\tau_0 = (1.57 \pm 0.45) \times 10^{-12}$ s for the high-temperature signal. The temperature at which the dynamic process is sufficiently slow as $\nu = 10^{-4}$ Hz (i.e., τ becomes hours) should be related to the soft–hard switching temperature (T_f). The temperatures were estimated to be 8.5 and 10.1 K for the low- and high-temperature signals, respectively, being consistent with the observation of the RM and ZFCM relaxation (Figure 4b). Owing to the overlap of two signals, the Cole–Cole diagram[22] did not show clear half circles.

A quantitative indicator for the soft and hard characters is the coercivity, which can be measured as a coercive field (H_C), or a hysteresis width, in the M–H curves. As Figure 5b shows, the magnetization of **p-5** almost saturated to a value of 9.21×10^3 erg Oe^{-1} mol^{-1} at 9 T, which satisfactorily agrees with a residual moment from the ferrimagnetic Co and NN spins. Below 10 K, **p-5** behaved as a very hard magnet showing a wide hysteresis loop. A coercive field (H_C) was as large as 51 kOe at 6 K, being comparable with the record coercivity of **p-4** (52 kOe at 6 K).[15] Interestingly, the coercive field is

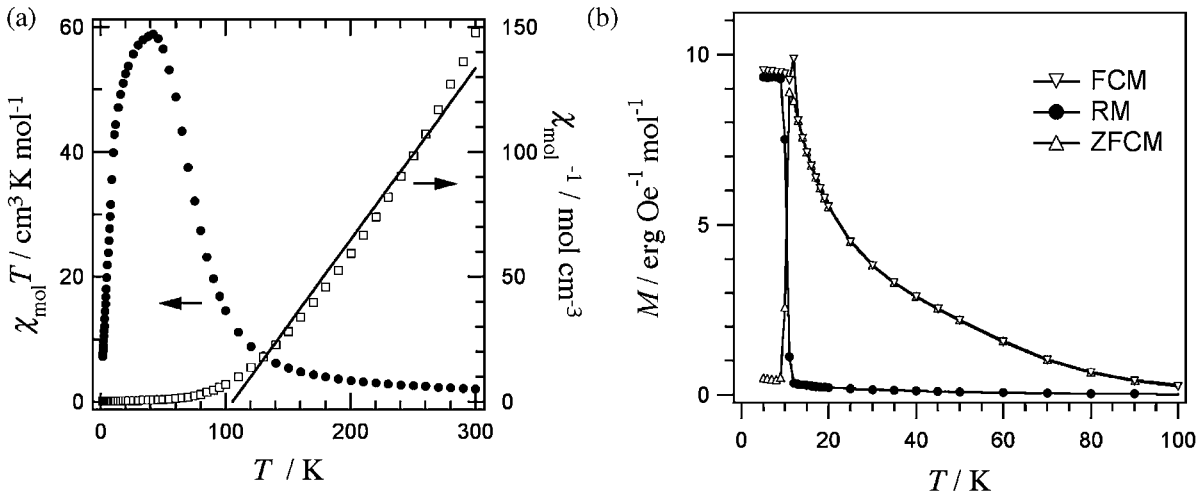

Figure 6. (a) The $\chi_{mol}T$ vs. T and χ_{mol}^{-1} vs. T plots for randomly oriented polycrystalline **o-3** with an applied field of 500 Oe. The Curie–Weiss analysis is indicated with a solid line. (b) FCM, RM, and ZFCM for polycrystalline **o-3** with an applied field of 5 Oe for FCM and ZFCM.

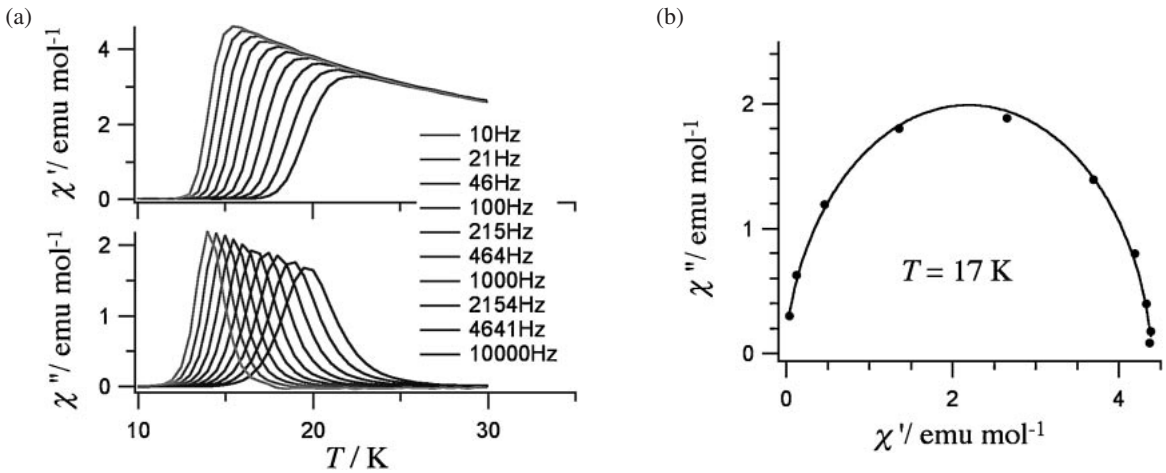

Figure 7. (a) Ac magnetic susceptibilities χ' and χ'' of polycrystalline **o-3** as a function of temperature and frequency. The ac field amplitude was 5 Oe. (b) The Cole–Cole plot of **o-3** measured at 17 K. A solid line represents calculation with $\alpha = 0.066$.

sensitive to temperature, and moreover we found the sweep rate dependence, suggesting again that the growth of the magnetic hardness is related to the freezing of the dynamics of magnetization reorientation. In contrast, above 15 K, the magnetization became typical of a soft magnet; the curve at 40 K exhibited a sharp rectangular S-shape without any hysteresis (the coercive field was less than a few Oe).

Therefore, we can summarize the results on **p-5** at this stage: the coercivity drastically changed across T_f, as a result of the slow or fast magnetization reorientation. Such hardness seems to require a long-range magnetic ordering.[15,16] The term of the freezing temperature, T_f, is used here instead of the blocking temperature, T_B, because the boundary of the present magnetic states involves a bulk phenomena and cannot be attributed solely to a single-molecule or single-chain origin. It would be a better way to use "freezing" (or melting, solidifying, glassifying, liquefying, etc.) for cooperative phenomena, and accordingly we avoided the term "blocking." The cooperative magnetization reorientation will be discussed later.

The magnetic properties of **p-2** and **p-3** have been investigated. Preliminary results of the magnetization measurements are shown in Figure 1S (Supporting Information). No appreciable hysteresis was observed. Details cannot be stated at present, because the crystal structures have not been determined so far.

Magnetic Properties of the Ortho-Derivatives. We measured magnetic properties of **o-3** and **o-5** according to the same methodology on the same apparatus as those of **p-5**. Figures 6 and 7 show the results of **o-3** and Figures 2S and 3S of **o-5** (Supporting Information). Ferrimagnetic chains were confirmed by the $\chi_{mol}T$ upsurge on cooling in the $\chi_{mol}T$ vs. T plots. The Curie–Weiss analysis on the data at 100–300 K gave the parameters C and θ (Table 2). The FCM, RM, and ZFCM experiments on **o-3** and **o-5** clarified hard and soft magnet behaviors below and above 10 K, respectively.

The classical dipolar coupling among the chains depends on the direction of the magnetic easy and hard axes, which is important for the bulk properties.[23] Fortunately, **o-2** gave

Table 2. Characteristics Values of the Magnetic Properties on **p-4**, **p-5**, **o-2**, **o-3**, and **o-5**

	Compounds				
	p-4	**p-5**[a)]	**o-2**	**o-3**	**o-5**
C/cm^3 K mol^{-1} [b)]	1.58	1.90 ± 0.01	1.71 ± 0.03	1.46 ± 0.04	1.74 ± 0.03
θ/K[b)]	83	87.2 ± 0.7	106 ± 2	109 ± 3	101 ± 2
ϕ[c)]	0.12	0.115 ± 0.003 (l) 0.113 ± 0.005 (h)	0.133 ± 0.009	0.121 ± 0.005	0.127 ± 0.004
α[d)]	0.251 (17 K)	—	0.138 ± 0.009 (20 K)	0.066 ± 0.010 (17 K)	0.19 ± 0.03 (20 K)
$E_a k_B^{-1}$/K	350 ± 6	290 ± 3 (l) 350 ± 5 (h)	357 ± 10	333 ± 6	360 ± 4
τ_0/10^{-12} s	0.68	2.15 ± 0.45 (l) 1.57 ± 0.45 (h)	3.3 ± 1.8	0.68 ± 0.27	1.02 ± 0.19
T_f/K[e)]	10	8.5 (l) 10.1 (h)	10.6	9.4	10.3
H_C/kOe[f)]	52 (6 K)	51 (6 K)	54 (6 K)	51 (5 K)	50 (6 K)
M_S/erg Oe^{-1} mol^{-1} [g)]	8 × 10^3	9.21 × 10^3	8.38 × 10^3	7.70 × 10^3	8.15 × 10^3
Reference	Ref. 15	this work	Ref. 17	this work	this work

a) Symbols (l) and (h) indicate the analyses of the low and high temperature χ_{ac} signals, respectively. b) From the Curie–Weiss analysis using the data at 100–300 K. c) From the analysis of the following equation: $\phi = (\Delta T_p/T_p)/\Delta(\log \omega)$. For details, see the text. d) From the Cole–Cole analysis. The measurement temperature is indicated in parenthesis. e) From the Arrhenius analysis with $\nu = 10^{-4}$ Hz. f) The temperature where the hysteresis was recorded is indicated in parenthesis. g) Magnetization at 9 T and 40 K.

several large single crystals suitable for magnetic anisotropy measurements on a SQUID magnetometer. The magnetic easy axis was found to be located perpendicular to the chain direction, and the hard axis in the chain direction.[17] This situation is similar to the magnetic anisotropy of **p-4**.[15] They have the same 2_1 screw symmetry in the same space group $P2_1/n$. The powder XRD results showed that all of the present compounds (**p-4**, **p-5**, **o-2**, **o-3**, and **o-5**) were approximately isomorphous. Assuming that all the compounds would have the same magnetic anisotropy, this type of anisotropy favors dipolar ferromagnetic coupling among the chains. In sharp contrast, **p-1** has the magnetic easy axis in the chain direction.[4] Antiferromagnetic coupling among the chains can be expected in that case.

The ac magnetic measurements on **o-3** and **o-5** were performed, and distinct frequency dependence was obtained around 15 K (Figures 7a and 3Sa). The signal was single, and a half-circle was clearly drawn in the Cole–Cole plot[22] for each compound (Figures 7b and 3Sb). We applied the theoretical formula,[24] and the calculation curve well reproduced the experimental data. The obtained α value was small (0.066), guaranteeing the presence of the single relaxation pathway in these compounds. Similar measurement and analysis on **o-5** gave the α value of 0.19. The ϕ [$=(\Delta T_p/T_p)/\Delta(\log \omega)$] values were calculated to be 0.121 and 0.127 for **o-3** and **o-5**, respectively.

The Arrhenius analysis afforded the parameters E_a and τ_0. The E_a values are considerably large as 333 ± 6 and 360 ± 4 K for **o-3** and **o-5**, respectively. The extrapolation with $\nu = 10^{-4}$ Hz gave the critical temperatures (T_f) of 9.4, and 10.3 K, respectively. These parameters are summarized in Table 2.

Finally, the magnetic hardness of **o-3** and **o-5** was confirmed by the hysteresis curves (Figure 8). The result of **o-2** is also shown for comparison (Figure 8a). Considerably wide hysteresis curves were recorded below T_f, where T_f is consistent with the estimation from the Arrhenius analysis. The saturation magnetizations were comparable with those of **p-4** and **p-5**. The apparent saturation magnetizations at lower temperatures (typically below 5 K) were much smaller than those at higher temperatures. This tendency can be explained again by the hard properties; the magnetic domain structures are frozen, so that the magnetization cannot reach the ideal saturation value at such low temperatures even when the field of 9 T was applied. Regardless of the alkyl positions (ortho and para), the magnetic properties are quite similar to each other (Figures 5b and 8).

Tunneling is observed at zero field for **o-2**. To clarify the presence of additional relaxation below T_f, the remnant magnetization decay was recorded as a function of time for **o-2**.[17] The rate constants were calculated according to the stretched exponential function.[20,25] The magnetization relaxation was found to be somewhat faster than the expectation from the Arrhenius behavior determined by means of the ac susceptometry,[17] which may be attributed to quantum tunneling of the magnetization.[20,26] Below T_f, tunneling is more significant at lower temperatures. Similar relaxation acceleration has been reported for several SMMs and SCMs.[27] The step at zero-field is significant for **o-2** but very moderate for **o-3** and **o-4**. Such difference seems to originate in the efficiency of tunneling, which depends on the internal bias field due to dipolar coupling and/or exchange coupling among the chains. That is, a molecular field is superposed on an applied field, leading to prohibition of tunneling at the nominally zero-applied field.

The coercive fields (H_C) were very large as 54 kOe (6 K) for **o-2**, 51 kOe (5 K) for **o-3**, and 50 kOe (6 K) for **o-5**. The present compounds belong to the hardest magnets ever reported.

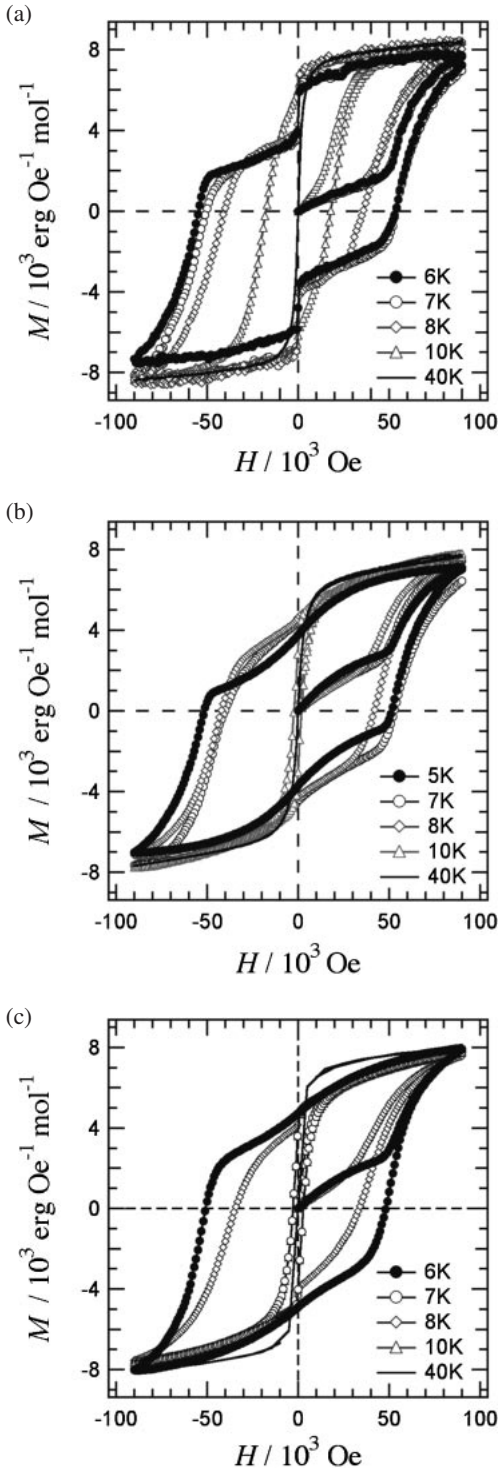

Figure 8. Hysteresis loops of polycrystalline specimens of (a) **o-2**, (b) **o-3**, and (c) **o-5**. Measurement temperatures are indicated. The field scan rate was almost constant at 18 Oe s^{-1}.

Furthermore, **o-2** has been proven to be a new record holder. The H_C was 54 kOe (4.1 MA m^{-1}) at 6 K of **o-2** is much larger than those of the molecule-based [MnTBrPP][TCNE]·2(CH_2Cl_2) (27.8 kOe at 2 K as the largest value before our work)[28] and even commercial permanent magnets $SmCo_5$ (44 kOe at room temp.) and $Nd_2Fe_{14}B$ (19 kOe at room temp.).[29]

Mechanism of the Arrhenius Behavior. At the boundary between the hard and soft magnet phases, there seems to be bulk (suggested by the giant coercivity) as well as the SCM character (suggested by the χ_{ac} frequency dependence). However, the μSR experiments on **p-4** revealed that the critical temperature for the hard magnetic phase was not an intrinsic characteristics value but largely dependent on the time scale of experimental tools to see the stabilization of the hard magnet state. The boundary is shifted to higher temperature as the time scale is shorter (28 K in μSR, 20–15 K in χ_{ac}, and 10 K in SQUID), according to a single Arrhenius behavior.[16] The intrinsic phase transition temperature has been suggested to be 40 K.[16] Muon facilities are rather limited, and we have not yet performed muon relaxation or rotation experiments for other derivatives. From the similarity of the structure and magnetism characterized for all the present compounds, we assume that the following discussion would hold also for **p-5**, **o-2**, **o-3**, and **o-5**.

If a SCM was formed first, and interchain coupling grew second, it would be normal. However, the present study works the other way around; magnetic ordering seems to take place first, and a SCM-like behavior second. We propose that the χ_{ac} frequency dependence would originate in the motion of the magnetic domain wall with an appreciable E_a. It seems to be reasonable to think that the domain wall motion takes place where the specimen has already undergone long-range order.

The E_a of the wall motion has the same origin of the magnetic anisotropy as the magnetization reorientation of each component (Figure 9a). In a single-chain magnet, the component corresponds to a monomeric spin carrier. We assume that a "kink" between two opposite magnetizations would move along the chain. The E_a is related with the nearest-neighbor exchange interaction, as originally suggested by Glauber.[30] However, the E_a values of the present compounds are as large as 300 K, much larger than those of the known SCMs[4–8] ($E_a/k_B = 154 \pm 2$ K[4] or 72 ± 1 K[7] for instance). The observation of the large E_a indicates that the interchain interaction should be taken into account. In a bulk magnet, each component in Figure 9a corresponds to a magnetic chain. The magnetic domain walls have a fairly large volume, and magnetization reversal of each chain takes place within a wall width in a collective manner, giving rise to a macroscopic wall motion with a considerable E_a.

Therefore, we can imagine a model for the domain wall motion in a long-range ordered state (Figure 9b). When a wall moves upward or downward in this figure, a kink in each chain moves to the left or the right side along the chain. In the presence of interchain ferromagnetic coupling, kinks move cooperatively so that the interchain nearest-neighbor correlation should remain ferromagnetic. In short, the kinks are bundled across chains to form a domain wall having dimensionality. The large E_a values are interpreted in terms of the combination of the intrinsic SCM E_a and the interchain dipolar ferromagnetic coupling. The latter coupling is rationalized by the fact that the easy axis is located perpendicular to the chain.[31]

Baranov et al. reported the slow dynamics of the magnetization in the ordered state of the manganese(II)–radical-based chain magnet.[32] The domain wall motion was investigated in connection with the low dimensional structure, and the E_a of

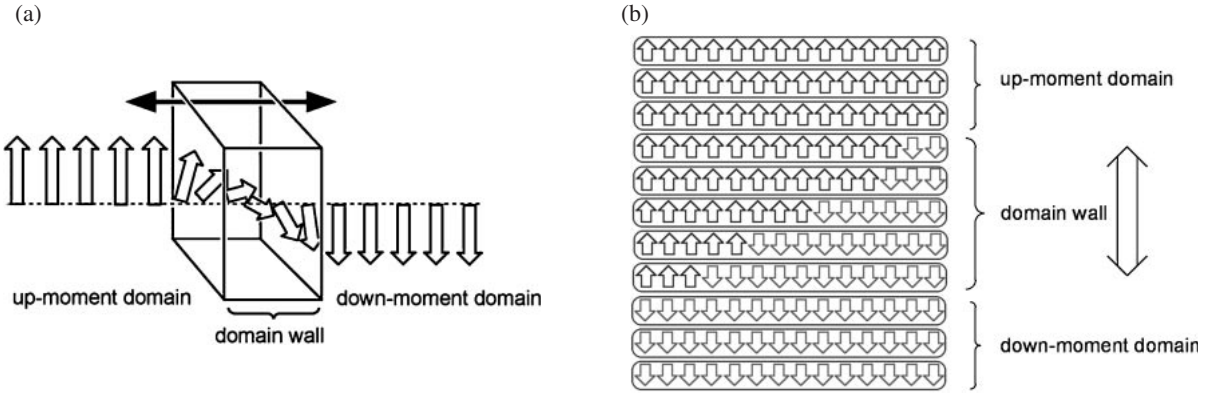

Figure 9. (a) A model for a magnetic domain wall motion. (b) The wall moves upward or downward, accompanied by magnetization reorientation on each chain. Only the cobalt spins in the ferrimagnetic Co–radical chains are drawn for clarity.

the domain wall motion was analyzed as the superposition of two contributions parallel and perpendicular to the chain directions. The term "glass" is usually used for the frozen spin systems consisting of single ions or molecules, but Coronado et al. reported the glassy behavior for motion of the magnetic domain wall in the hexacyanoferrate(III)-based layered magnet.[33] Inoue et al. reported similar behavior observed in a cobalt(II)–biradical chain.[34] Miller et al. also reported the glassy behavior of the [MnTPP][TCNE] series from manganese(III) tetraphenylporphyrinate and tetracyanoethylene, and the large H_C observed was attributed to the magnetically ordered state.[23]

The mechanism on the magnetic ordered state of **p-4** has recently been argued on the basis of the ac susceptibility results together with the μSR experiments.[16] Similarly, the magnetically ordered state of all the present compounds (Table 2) can be interpreted as follows. The magnetic hardness very gradually grows in a unique phase below the intrinsic magnetic phase transition around 40 K. Although the spins tend to form the long-range ordered state, moving domain walls disturb the alignment of the spins. The considerably large E_a brings about the drastic slowing-down of the dynamics. On cooling, the dynamics of domain walls become more static to be observable in the ac magnetic susceptibility, and the hard magnet state is finally settled down below 10 K. The large E_a is effective for the drastically increasing H_C owing to the freezing domain wall motion. The presence of the sizable interchain coupling also leads to the relatively high T_N. Therefore, the classical dipolar coupling plays an important role in increasing H_C as well as elevating T_N (T_C).

Summary

We can draw the "phase" diagram of the present compounds listed in Table 2 as follows: a hard magnet at $T \leq T_f$, a soft magnet at $T_f < T \leq T_C$, and a paramagnet at $T_C < T$. Thus, they can be regarded as novel hard–soft-switchable magnets, simply by means of heating and cooling across T_f. The H_C and E_a belong to the largest class among those of the known compounds. The interplay between SCM and bulk characters has been found, which originates in ferromagnetic assembly of the single-chain magnets. The classical dipolar coupling is versatile both for the development of high T_N (T_C) and high H_C magnets. To the best of our knowledge, the family of [Co(hfac)$_2$(C$_n$PNN)] is the record holder of the largest coercive field among hard magnets ever known. The preparation of a new class of magnets [Co(hfac)$_2$(C$_n$PNN)] and observation of their hard property have been thus generalized.

Experimental

Materials. Dark bluish purple crystalline radicals *p*-C_5PNN, *o*-C_2PNN, *o*-C_3PNN, and *o*-C_5PNN were prepared from the corresponding aldehydes according to the Ullman procedure.[1] The following procedure is typical.

A methanol solution (50 mL) containing 7.50 g (50 mmol) of *o*-ethoxybenzaldehyde and 7.40 g (50 mmol) of 2,3-dimethyl-2,3-bis(hydroxylamino)butane[35] was stirred at room temperature under nitrogen atmosphere for 2 days. After addition of water (300 mL), the resultant colorless solid was collected on a filter and dried to give the precursor dihydroxyimidazoline. An aqueous solution (100 mL) of $NaIO_4$ (11.4 g, 53.3 mmol) was added to a mixture of 10.0 g (35.7 mmol) of the above precursor in water (100 mL) at room temperature while being stirred. The mixture immediately turned purple. After the reaction was completed by monitoring with thin-layer chromatography, 300 mL of CH_2Cl_2 was added and the organic layer was separated. The resultant solution was dried over anhydrous $MgSO_4$, concentrated under reduced pressure, and purified by silica gel column chromatography eluted with a 1/1 dichloromethane–ether mixed solution. A purple fraction was collected and concentrated under reduced pressure. Recrystallization from a mixed solvent of 1/1 dichloromethane–ether gave 2.50 g (9.0 mmol) of *o*-C_2PNN as a fine purple crystalline solid. Yield: 25%. Mp: 108–110 °C. Anal. Calcd for $C_{15}H_{21}N_2O_3$: C, 64.96; H, 7.63; N, 10.10%. Found: C, 65.26; H, 7.67; N, 9.12%. ESR (toluene, room temp.): $g = 2.0066$, $a_N = 7.58$ G. MS (EI): m/z, 277 (M^+). IR (KBr disc): 2983, 2935, 2883, 1602, 1529, 1473, 1400, 1369, 1284, 1253, 1145, 1116, 1039, 925, 871, 767, 540 cm^{-1}.

Compound *p*-C_5PNN was prepared according to the procedure for *p*-C_4PNN.[10] Data for *p*-C_5PNN are as follows: Yield: 23%. Mp: 81–83 °C. Anal. Calcd for $C_{18}H_{27}N_2O_3$: C, 67.68; H, 8.52; N, 8.77%. Found: C, 67.42; H, 8.69; N, 8.57%. ESR (toluene, room temp.): $g = 2.0065$, $a_N = 7.55$ G. MS (EI): m/z 318.2 (M^+). IR (KBr disc): 1537, 1386, 1255, 1020 cm^{-1}.

Compounds *o*-C_3PNN and *o*-C_5PNN were prepared according to the procedure for *o*-C_2PNN. Data for *o*-C_3PNN are as follows: Yield: 14%. Mp: 119–120 °C. Anal. Calcd for $C_{16}H_{23}N_2O_3$: C, 65.96; H, 7.96; N, 9.61%. Found: C, 66.11; H, 7.55; N, 9.88%. ESR (toluene, room temp.): $g = 2.0066$, $a_N = 7.50$ G. MS (EI): m/z 291 (M^+). IR (KBr disc): 2960, 2910, 2879, 1604, 1535, 1469, 1444, 1402, 1369, 1295, 1247, 1159, 1135, 1106, 1043, 1016, 873, 757, 539 cm^{-1}. Data for *o*-C_5PNN are as follows: Yield: 27%. Purple oil. Anal. Calcd for $C_{18}H_{27}N_2O_3$: C, 67.68; H, 8.52; N, 8.77%. Found: C, 67.24; H, 8.73; N, 7.44%. ESR (toluene, room temp.): $g = 2.0066$, $a_N = 7.50$ G. MS (ESI): m/z 341 ($M + Na^+$). IR (KBr disc): 2989, 2952, 2871, 1608, 1537, 1488, 1403, 1363, 1288, 1255, 1172, 1137, 1041, 985, 873, 752, 536 cm^{-1}.

A heptane solution (40 mL) containing $[Co(hfac)_2]\cdot 2H_2O$ (250 mg; 0.50 mmol) was refluxed, concentrated until the volume was decreased to ca. 5 mL, and cooled to room temperature. A dichloromethane solution (2 mL) containing *o*-C_2PNN (162 mg, 0.51 mmol) was added to the above solution. The resultant solution was allowed to stand in a refrigerator, to give fine bluish purple needles of $[Co(hfac)_2(o\text{-}C_2PNN)]$ (**o-2**) (180 mg, 0.24 mmol) in 48% yield. Mp: 114–115 °C. Anal. Calcd for $C_{25}H_{23}CoF_{12}N_2O_7$: C, 40.02; H, 3.09; N, 3.73%. Found: C, 39.75; H, 2.84; N, 3.80%. IR (KBr disc): 1646, 1255, 1205, 1145, 792, 754, 667, 586, 536 cm^{-1}.

Compounds **o-3**, **o-5**, and **p-5** were prepared according to the method for **o-2** and **p-4**.[10] Data on these derivatives are as follows. $[Co(hfac)_2(p\text{-}C_5PNN)]$ (**p-5**): Yield: 34%. Mp: 98–102 °C. Anal. Calcd for $C_{28}H_{29}CoF_{12}N_2O_7$: C, 42.44; H, 3.69; N, 3.54%. Found: C, 42.52; H, 3.44; N, 3.74%. IR (KBr disc): 1643, 1552, 1386, 1340, 1255, 1020 cm^{-1}. $[Co(hfac)_2(o\text{-}C_3PNN)]$ (**o-3**): Yield: 42%. Mp: 119–120 °C. Anal. Calcd for $C_{26}H_{25}CoF_{12}N_2O_7$: C, 40.85; H, 3.30; N, 3.66%. Found: C, 42.52; H, 3.44; N, 3.74%. IR (KBr disc): 1648, 1257, 1199, 1145, 790, 752, 667 cm^{-1}. $[Co(hfac)_2(o\text{-}C_5PNN)]$ (**o-5**): Yield: 33%. Mp: 117–118 °C. Anal. Calcd for $C_{28}H_{29}CoF_{12}N_2O_7$: C, 42.44; H, 3.69; N, 3.54%. Found: C, 41.62; H, 3.46; N, 3.16%. IR (KBr disc): 1646, 1257, 1203, 1145, 792, 754, 667, 584, 538 cm^{-1}.

X-ray Crystallographic Analysis. Diffraction data of a single crystal of **p-5** were collected on a Rigaku R-axis RAPID diffractometer with graphite monochromated Mo Kα radiation. The structure was directly solved, and the parameters were refined using all the data. CCDC 756165 contains the supplementary crystallographic data for **p-5**. These data can be obtained free of charge from The Cambridge Crystallographic Data Centre via www.ccdc.cam.ac.uk/data_request/cif. Powder X-ray diffraction data were collected on a Rigaku Ultima III diffractometer with graphite monochromated Cu Kα radiation ($\lambda = 1.5418$ Å) at 300 K.

Magnetic Measurements. Dc magnetic susceptibilities and static magnetizations of the polycrystalline samples were measured down to 1.8 K on a Quantum Design MPMS SQUID magnetometer equipped with a 7 T coil. The magnetic response was corrected with diamagnetic blank data of the sample holder obtained separately. The diamagnetic contribution of the sample itself was estimated from Pascal's constant. Ac magnetic susceptibilities were obtained with 5 Oe ac fields (10–10^4 Hz) at zero dc field in a temperature range down to 2.0 K on a Quantum Design PPMS ac/dc magnetometer with a 9 T coil. Hysteresis curves in ±9 T were recorded on the PPMS magnetometer.

This work was partly supported by Grants-in-Aid for Scientific Research (Nos. 19550135, 21110513, and 22350059) from the Ministry of Education, Culture, Sports, Science and Technology, Japan and by a research grant from the Japan Securities Scholarship Foundation.

Supporting Information

Figures 1S–3S for selected magnetic data on **p-2**, **p-3**, and **o-5**. This material is available electronically on the web at http://www.csj.jp/journals/bcsj/.

References

1 E. F. Ullman, J. H. Osiecki, D. G. B. Boocock, R. Darcy, *J. Am. Chem. Soc.* **1972**, *94*, 7049.

2 a) A. Caneschi, D. Gatteschi, R. Sessoli, P. Rey, *Acc. Chem. Res.* **1989**, *22*, 392. b) A. Caneschi, D. Gatteschi, P. Rey, *Prog. Inorg. Chem.* **1991**, *39*, 331.

3 D. Gatteschi, R. Sessoli, J. Villain, *Molecular Nanomagnets*, Oxford University Press, New York, **2006**.

4 A. Caneschi, D. Gatteschi, N. Lalioti, C. Sangregorio, R. Sessoli, G. Venturi, A. Vindigni, A. Rettori, M. G. Pini, M. A. Novak, *Angew. Chem., Int. Ed. Engl.* **2001**, *40*, 1760.

5 N. Ishii, T. Ishida, T. Nogami, *Inorg. Chem.* **2006**, *45*, 3837.

6 a) L. Bogani, C. Sangregorio, R. Sessoli, D. Gatteschi, *Angew. Chem., Int. Ed.* **2005**, *44*, 5817. b) K. Bernot, L. Bogani, A. Caneschi, D. Gatteschi, R. Sessoli, *J. Am. Chem. Soc.* **2006**, *128*, 7947.

7 R. Clérac, H. Miyasaka, M. Yamashita, C. Coulon, *J. Am. Chem. Soc.* **2002**, *124*, 12837.

8 a) T.-F. Liu, D. Fu, S. Gao, Y.-Z. Zhang, H.-L. Sun, G. Su, Y.-J. Liu, *J. Am. Chem. Soc.* **2003**, *125*, 13976. b) E. Pardo, R. Ruiz-García, F. Lloret, J. Faus, M. Julve, Y. Journaux, F. Delgado, C. Ruiz-Pérez, *Adv. Mater.* **2004**, *16*, 1597. c) N. E. Chakov, W. Wernsdorfer, K. A. Abboud, G. Christou, *Inorg. Chem.* **2004**, *43*, 5919. d) L. M. Toma, R. Lescouëzec, J. Pasán, C. Ruiz-Pérez, J. Vaissermann, J. Cano, R. Carrasco, W. Wernsdorfer, F. Lloret, M. Julve, *J. Am. Chem. Soc.* **2006**, *128*, 4842. e) H. Miyasaka, T. Madanbashi, K. Sugimoto, Y. Nakazawa, W. Wernsdorfer, K.-i. Sugiura, M. Yamashita, C. Coulon, R. Clérac, *Chem.—Eur. J.* **2006**, *12*, 7028. f) A. Okazawa, T. Nogami, H. Nojiri, T. Ishida, *Chem. Mater.* **2008**, *20*, 3110.

9 a) W. Wernsdorfer, N. Aliaga-Alcalde, D. N. Hendrickson, G. Christou, *Nature* **2002**, *416*, 406. b) H. Miyasaka, K. Nakata, L. Lecren, C. Coulon, Y. Nakazawa, T. Fujisaki, K.-i. Sugiura, M. Yamashita, R. Clérac, *J. Am. Chem. Soc.* **2006**, *128*, 3770.

10 C. Benelli, A. Caneschi, D. Gatteschi, R. Sessoli, *Inorg. Chem.* **1993**, *32*, 4797.

11 T. Ise, T. Ishida, D. Hashizume, F. Iwasaki, T. Nogami, *Inorg. Chem.* **2003**, *42*, 6106.

12 K. Inoue, H. Iwamura, *Chem. Commun.* **1994**, 2273.

13 J. S. Miller, J. C. Calabrese, R. S. McLean, A. J. Epstein, *Adv. Mater.* **1992**, *4*, 498.

14 V. N. Ikorskii, V. I. Ovcharenko, Y. G. Shvedenkov, G. V. Romanenko, S. V. Fokin, R. Z. Sagdeev, *Inorg. Chem.* **1998**, *37*, 4360.

15 N. Ishii, Y. Okamura, S. Chiba, T. Nogami, T. Ishida, *J. Am. Chem. Soc.* **2008**, *130*, 24.

16 T. Ishida, Y. Okamura, I. Watanabe, *Inorg. Chem.* **2009**, *48*, 7012.
17 Y. Okamura, T. Nogami, T. Ishida, *Chem. Lett.* **2009**, *38*, 740.
18 a) D. C. Jiles, *Acta Mater.* **2003**, *51*, 5907. b) A. Inoue, *Mater. Sci. Eng. A* **1997**, *226–228*, 357. c) J. M. D. Coey, *J. Alloys Compd.* **2001**, *326*, 2.
19 a) W. Hibbs, D. K. Rittenberg, K.-i. Sugiura, B. M. Burkhart, B. G. Morin, A. M. Arif, L. Liable-Sands, A. L. Rheingold, M. Sundaralingam, A. J. Epstein, J. S. Miller, *Inorg. Chem.* **2001**, *40*, 1915. b) D. Gatteschi, R. Sessoli, J. Villain, *Section 3.1.5 Ac susceptometry* in *Molecular Nanomagnets*, pp. 69–75 in Ref. 3.
20 D. Gatteschi, R. Sessoli, *Angew. Chem., Int. Ed.* **2003**, *42*, 268.
21 S. M. J. Aubin, Z. Sun, L. Pardi, J. Krzystek, K. Folting, L.-C. Brunel, A. L. Rheingold, G. Christou, D. N. Hendrickson, *Inorg. Chem.* **1999**, *38*, 5329.
22 K. S. Cole, H. R. Cole, *J. Chem. Phys.* **1941**, *9*, 341.
23 C. M. Wynn, M. A. Gîrtu, W. B. Brinckerhoff, K.-i. Sugiura, J. S. Miller, A. J. Epstein, *Chem. Mater.* **1997**, *9*, 2156.
24 R. Sessoli, A. K. Powell, *Coord. Chem. Rev.* **2009**, *253*, 2328.
25 L. Thomas, A. Caneschi, B. Barbara, *Phys. Rev. Lett.* **1999**, *83*, 2398.
26 a) D. Gatteschi, L. Pardi, A. L. Barra, A. Müller, J. Döring, *Nature* **1991**, *354*, 463. b) G. Christou, D. Gatteschi, D. N. Hendrickson, R. Sessoli, *MRS Bull.* **2000**, *25*, No. 11, 66.
27 a) M. A. Novak, W. S. D. Folly, J. P. Sinnecker, S. Soriano, *J. Magn. Magn. Mater.* **2005**, *294*, 133. b) M. Ferbinteanu, H. Miyasaka, W. Wernsdorfer, K. Nakata, K.-i. Sugiura, M. Yamashita, C. Coulon, R. Clérac, *J. Am. Chem. Soc.* **2005**, *127*, 3090. c) E.-C. Yang, W. Wernsdorfer, L. N. Zakharov, Y. Karaki, A. Yamaguchi, R. M. Isidro, G.-D. Lu, S. A. Wilson, A. L. Rheingold, H. Ishimoto, D. N. Hendrickson, *Inorg. Chem.* **2006**, *45*, 529.
28 a) D. K. Rittenberg, K.-i. Sugiura, Y. Sakata, S. Mikami, A. J. Epstein, J. S. Miller, *Adv. Mater.* **2000**, *12*, 126. b) A. J. Epstein, *MRS Bull.* **2000**, *25*, No. 11, 33.
29 J. Fidler, T. Schrefl, S. Hoefinger, M. Hajduga, *J. Phys.: Condens. Matter* **2004**, *16*, S455.
30 R. J. Glauber, *J. Math. Phys.* **1963**, *4*, 294.
31 R. Sessoli, *Angew. Chem., Int. Ed.* **2008**, *47*, 5508.
32 N. V. Baranov, N. V. Mushnikov, T. Goto, Y. Hosokoshi, K. Inoue, *J. Phys.: Condens. Matter* **2003**, *15*, 8881.
33 E. Coronado, C. J. Gómez-García, A. Nuez, F. M. Romero, J. C. Waerenborgh, *Chem. Mater.* **2006**, *18*, 2670.
34 Y. Numata, K. Inoue, N. Baranov, M. Kurmoo, K. Kikuchi, *J. Am. Chem. Soc.* **2007**, *129*, 9902.
35 M. Lamchen, T. W. Mittag, *J. Chem. Soc. C* **1966**, 2300.